Determining binding energies of valence-band electrons in insulators and semiconductors via lanthanide spectroscopy

Pieter Dorenbos

Luminescence Materials Research group, Department of Radiation Science and Technology, Faculty of Applied Sciences, Delft University of Technology, Mekelweg 15, 2629 JB Delft, Netherlands

(Received 20 April 2012; revised manuscript received 27 July 2012; published 14 January 2013)

Models and methods to determine the absolute binding energy of $4f$-shell electrons in lanthanide dopants will be combined with data on the energy of electron transfer from the valence band to a lanthanide dopant. This work will show that it provides a powerful tool to determine the absolute binding energy of valence band electrons throughout the entire family of insulator and semiconductor compounds. The tool will be applied to 28 fluoride, oxide, and nitride compounds providing the work function and electron affinity together with the location of the energy levels of all divalent and all trivalent lanthanide dopants with an accuracy that surpasses that of traditional methods like photoelectron spectroscopy. The 28 compounds were selected to demonstrate how work function and electron affinity change with composition and structure, and how electronic structure affects the optical properties of the lanthanide dopants. Data covering more than 1000 different halide (F, Cl, Br, I), chalcogenide (O, S, Se), and nitride compounds are available in the archival literature enabling us to routinely establish work function and electron affinity for this much wider collection of compounds.

DOI: 10.1103/PhysRevB.87.035118 PACS number(s): 71.23.An, 78.20.−e, 78.55.−m

I. INTRODUCTION

The electronic structure of insulators and semiconductors together with the location of impurity states within the band gap are crucial for the performance of impurity activated compounds as functional materials.[1–4] Traditionally, photoelectron spectroscopy techniques are used to determine the electron binding energies in the upper band states of compounds.[2,5–7] It requires ultrahigh vacuum and the properties close to the surface are probed. One has to deal with surface effects, sample charging, contact potentials, and limited resolution leading to substantial systematic and random error. Band structure calculations are also not at a level to accurately, say within a few 0.1 eV, determine electron binding energies. Yet such information is highly desired. For example, in semiconductor technology, knowledge on electron and hole transfer across a heterojunction is important. The valence and conduction band offsets (VBO and CBO) at the interface then play an important role.[8] To reduce gate leakage currents, high dielectric constant oxides are needed to replace SiO_2 in complementary metal oxide silicon (CMOS) transistors.[9,10] The CB offset with Si is one of the key criteria in the selection of such replacement. Knowledge of the bulk electronic structure of oxides, particularly a model that predicts and relates band offsets with chemical trends, is required. The same applies in the field of solar hydrogen production by means of water splitting in photoelectrochemical cells (PEC) utilizing inorganic photoanodes; the anode conduction and valence band edges should "straddle" the reduction and oxidation potentials of water.[11,12]

The past decade has witnessed much progress in our understanding and modeling of the placement of the lanthanide energy levels with respect to the valence band in inorganic compounds.[2,3,13–15] Those models employ the wealth of data available on optical transitions between the host bands and lanthanide impurity states. In this work those models and data are combined with the chemical shift model that was presented in Ref. 16. The chemical shift model provides a method or a tool to determine the electron binding energies relative to the vacuum, i.e., it provides the minimum energy needed to bring an electron from an electronic state to the vacuum at infinite distance. Here we will demonstrate that the tool can be used throughout the entire family of inorganic compounds (halides, chalcogenides, pnictides) which then provides the work function and electron affinities on a routine basis. For this purpose 28 different compounds were selected to demonstrate that the results from the chemical shift model are fully consistent with information derived from other well established experimental techniques.

II. MODELS AND THEORY

Various empirical models, as reviewed in Ref. 15, were developed in the past 15 years to explain and predict the spectroscopic properties of divalent and trivalent lanthanide impurities in inorganic compounds. It turns out that those properties, i.e., the energy of electronic transitions within a lanthanide ion or between a lanthanide ion and the host valence and conduction bands, change in a very systematical and therewith predictable fashion with the number n of electrons in the $4f$ shell of such a lanthanide ion. Such systematical fashion can be conveniently illustrated with a so-called host referred binding energy (HRBE) scheme. Figure 1, with the right-hand energy scale, shows the HRBE of $4f$-shell electrons of all divalent and all trivalent lanthanide ions in YPO_4.[16] The ground state $4f$-shell electron binding energies, or equivalently the $Ln^{2+/3+}$ or $Ln^{3+/4+}$ donor/acceptor level locations, follow characteristic double zigzag curves with an increase in the number n of electrons in the $4f$ shell. The lower double zigzag curve connects the ground state energy of the trivalent lanthanides and the upper one of the divalent ones. When ground state energies are known, the rich level scheme of excited $4f$ states can also be drawn. The scheme shows for example that the ground state of Ce^{3+} ($n = 1$) is located 3.8 eV above the top of the valence band E_V. This means that the electron at the top of the valence band is 3.8 eV

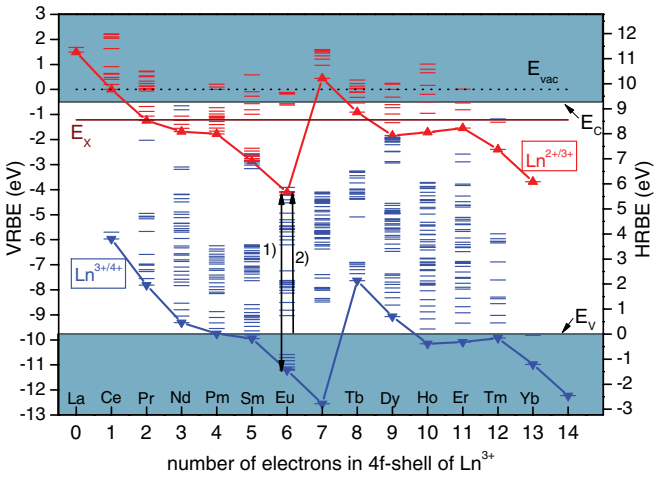

FIG. 1. (Color online) Scheme with the location of divalent and trivalent lanthanide impurity $4f$ levels in YPO_4. The left-hand scale shows the vacuum referred and the right-hand scale the host referred binding energies. Arrow 1 indicates the size of $U(6,YPO_4)$. Arrow 2 indicates electron transfer from the valence band top to Eu^{3+}.

more strongly bonded than an electron in the $4f$-ground state of Ce^{3+}, or in other words, it requires 3.8 eV more energy to remove an electron from the top of the valence band than from the $4f$ shell of Ce^{3+}.

The shapes of the two double zigzag curves are invariant within a few 0.1 eV through the entire family of inorganic compounds (halides, chalcogenides, and pnictides). This was evidenced by experimental data covering many different compounds,[3,13,16] and it was explained by the chemical shift model presented in Ref. 16. It implies that one only needs to pin the $4f$-shell electron binding energy for one divalent (usually Eu^{2+}) and one trivalent (usually Ce^{3+}) lanthanide relative to the valence band to construct such a HRBE scheme with the binding energies in all lanthanide impurity ground and excited states.

To construct a vacuum referred binding energy (VRBE) scheme with the left-hand energy scale in Fig. 1 is quite a different challenge. One needs to establish the absolute binding energy of just one of the electronic HRBE states to pin the entire scheme. However, accuracy to establish this by either experiment or theory appears poor. The chemical shift model presented in Ref. 16 relates the energy difference $U(6,A)$ between the $4f$-shell electron binding energies $E_{4f}(7,2+,A)$ in Eu^{2+} and $E_{4f}(6,3+,A)$ in Eu^{3+} (see arrow 1 in Fig. 1) with the absolute binding energy $E_{4f}(7,2+,A)$. The idea is very simple. Due to the Coulomb repulsion between a $4f$-shell electron in Eu^{2+} and the negative charge of the surrounding anion ligands, the $4f$-shell electron binding energy in Eu^{2+} is shifted towards weaker bonding with respect to the binding energy $E_{4f}(7,2+,\text{vacuum}) = -24.92$ eV in the free (gaseous) ion. This chemical shift for Eu^{2+} appears smaller than that for Eu^{3+} simply because the effective negative screening charge around Eu^{2+} is one third smaller than that around Eu^{3+}, and as a consequence the energy difference $U(6,A)$ has reduced. Experiment shows that it decreases from 18.05 eV in the free Eu ions, to 7.4 eV for Eu in aqueous solution, and to about 5.6 eV for Eu metal.[16]

Based on those ideas and data a relationship between the value for $U(6,A)$ and the size of the chemical shift was proposed which then gave

$$E_{4f}(7,2+,A) = -24.92 + \frac{18.05 - U(6,A)}{0.777 - 0.0353U(6,A)}, \qquad (1)$$

where all energies are in eV. -24.92 eV is the experimentally known $4f$-shell electron binding energy for gaseous Eu^{2+} (A = vacuum), and the second term on the right-hand side is the chemical shift. The constants 0.777 and 0.0353 were chosen to best reproduce the experimental $4f$-shell VRBE data for aqueous solutions of Eu, pure Eu metal, and Eu as dopant in LaF_3. In Ref. 16 it was suggested but not evidenced that the same equation with the same constants should apply to all chemical environments A alike. Here in this work that evidence will be provided by presenting and analyzing data on 28 different inorganic compounds with members from the wide band gap fluorides, the aluminium based oxides, and nitride compounds.

The value of $U(6,YPO4) = 7.1$ eV (see arrow 1 in Fig. 1) yields with Eq. (1), $E_{4f}(7,2+,A) = -4.1$ eV. This value then pins the entire HRBE scheme for YPO_4 to the vacuum level expressed by the left-hand energy scale in Fig. 1. $U(6,A)$ can be obtained from lanthanide spectroscopy and appears about 7.6 to 7.3 eV in poorly polarizable fluoride compounds, 7.3 to 6.5 eV in oxide compounds, and 6.3 to 6.1 eV in sulfide compounds.[17] Equation (1) then teaches that $E_{4f}(7,2+,A)$ varies from -4.4 eV in fluorides to -3.7 eV in sulfides. It is therefore quite invariant through the entire family of inorganic compounds. This finding shows much similarity with the *internal reference rule* for transition metal (TM) impurities[18,19] which states that within a class of similar compounds the VRBE of a TM-impurity d-electron ground state is nearly constant. Later the rule was proposed to apply also to the $4f$-electron ground states of lanthanide impurities.[20,21] However, the rule appeared not very strong and Malguth *et al.*[1] in their review on Fe impurity states in III-V and II-VI semiconductors concluded that the rule holds to a certain extent inside a materials group but between different materials groups it only provides a rough trend. Whereas the internal reference rule stems from experimental observation without further theoretical explanation or derivation, the chemical shift model generates Eq. (1) which actually explains why an internal reference rule should apply in some cases, but it also explains why it is bound to fail in other cases.

Knowledge on $E_{4f}(7,2+,A)$ pins the entire HRBE scheme and therefore provides a tool to determine the energy $E_V(A)$ at the top of the valence band. That same energy can be determined independently from photoelectron spectroscopy studies on the pure host compounds, and such data can then be used to validate Eq. (1). For $E_V(A)$, that is equivalent to the work function $\Phi(A)$, one may write

$$E_V(A) = E_{4f}(7,2+,A) - E^{CT}(6,3+,A) \equiv -\Phi(A), \qquad (2)$$

where $E^{CT}(6,3+,A)$ is the energy needed to bring an electron from the top of the valence band into the $4f$ shell of Eu^{3+} thus creating Eu^{2+}, see arrow 2 in Fig. 1. Such excitation is observed as the Eu^{3+} charge transfer (CT) band in Eu^{3+}

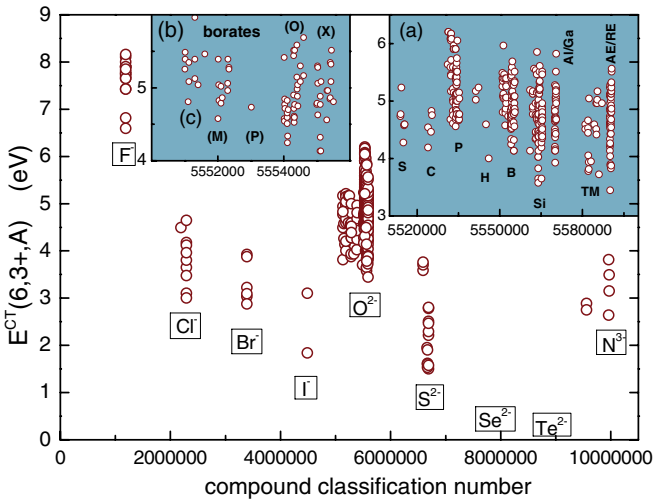

FIG. 2. (Color online) The energy $E^{CT}(6,3+,A)$ of electron transfer from the valence band to Eu^{3+} in about 500 different compounds against a seven-digit compound classification number. Inset (a) is an expanded view of the data on oxide compounds where data are grouped in sulfates (S), carbonates (C), phosphates (P), etc (TM is a transition metal, AE is an alkaline earth, and RE is a rare earth cation). Inset (b) is an expanded view of the data on borate compounds with from left to right a grouping in condensed (C), meta (M), pyro (P), otho (O), and oxy-ortho (X) borates.

luminescence excitation spectra. Much data on $E^{CT}(6,3+,A)$ are available in literature.[22] They have been gathered and are shown in Fig. 2 against a seven-digit compound classification number that reflects compositional and structural properties of the compound.[23] In fluoride compounds E^{CT} is largest, about 7–8 eV, and it decreases when going to chloride, bromide, and iodide compounds. Since $E_{4f}(7,2+,A)$ is relatively constant, this immediately demonstrates that $E^{CT}(7,2+,A)$ reflects variations in $E_V(A)$. The insets of Fig. 2 show an exploded part of the data on the oxides and the borate compounds, and it shows that both the chemistry and the structure of the compound affect the value of E^{CT}.

Once $E_V(A)$ is available, the energy $E_C(A)$ at the bottom of the conduction band is obtained with

$$E_C(A) = E_V(A) + 1.08 \times E^{ex}(A) \equiv -\chi(A), \qquad (3)$$

where $E^{ex}(A)$ is the energy of exciton creation in the host compound. As rule of thumb, $E_C(A)$ is assumed at 8% higher energy in order to account for the electron and hole binding energy in the exciton. The electron affinity $\chi(A)$ in Eq. (3) is equivalent to the binding energy at the bottom of the conduction band. Like for $E^{CT}(6,3+,A)$, data on $E^{ex}(A)$ are available on many hundreds of compounds, a large part of which was compiled in Ref. 22.

III. THE REQUIRED INPUT DATA

In order to construct a $4f$-VRBE scheme like in Fig. 1 using Eqs. (1), (2), and (3), one needs information on the three host dependent values $U(6,A)$, $E^{CT}(6,3+,A)$, and $E^{ex}(A)$. They are compiled in Table I for the 28 different compounds that were selected to evidence Eq. (1) and to demonstrate the potential of the tool presented. In determining E^{ex} one should take great care because it is very easily underestimated. Ideally, host exciton creation is evidenced by a distinct band in the excitation spectrum of intrinsic or excitonic emission of the pure host compound. However, compounds always contain impurities and defects, and excitons created near those defects may appear at several 0.1 eV of lower energy.

Excitation and emission bands narrow at low temperature, say 10 K, and this facilitates better identification of the host exciton band. When also time resolved excitation spectra are available, even better assignments can be made. Comparing excitation spectra of undoped and intentionally doped compounds with each other may further help in an unambiguous discrimination between genuine host excitonic bands, near defect excitonic bands, and defect excited states. All those methods were applied for the compounds in Table I in order to assign the proper value to $E^{ex}(A)$. Due to lattice expansion, the host exciton creation energy depends slightly on temperature; it tends to increase on cooling from room temperature to 10 K. In wide band gap compounds the shift can be as large as -1 meV/K, whereas in covalent semiconductors such as Si or Ge the shift appears smaller (-0.22 and -0.44 meV/K).[24] The listed values for E^{ex} pertain to the energy at the peak of the exciton creation band at low temperatures of typically 10 K. In the cases where only room temperature E^{ex} values were retrieved from literature, a $\approx$3% correction was made; those data are listed in italic font.

Information to deduce E^{ex} for GdF_3 was not found. The value of 10.9 eV in Table I is an educated guess based on a clear trend observed within the REF_3 compounds (RE = La, Y, Lu). E^{ex} increases with a smaller size of the rare earth cation of the REF_3 compound, and then the value for GdF_3 was obtained by interpolation. The E^{ex} values for the $LiREF_4$, $LiCaAlF_6$, and AEF_2 compounds (AE = alkaline earth = Ca, Sr, Ba) are all well established. n-type CdF_2 has its room temperature Γ-Γ exciton peak in reflectivity spectra at 7.6 eV from which a 10 K value of $\approx$7.8 is estimated. Like for the wide band gap fluorite compounds, vacuum ultraviolet spectroscopy is needed to derive E^{ex} for most wide band oxide compounds. The value listed for the magnetoplumbite $LaMgAl_{11}O_{19}$ is based on excitation spectra of Eu^{2+},[25,26] Mn^{2+},[27] and Pr^{3+} doped compounds[28] performed at room temperature. VUV studies on Pr^{3+} doped,[29] Mn^{2+} doped,[30] and Tb^{3+} and Ce^{3+} doped[31] $SrAl_{12}O_{19}$ reveal the host exciton band at 7.7 eV at room temperature and 7.9 eV at 10 K.

Column 4 in Table I lists the $E^{CT}(6,3+,A)$ CT energies as derived from or reported in the cited references. Information on the CT energy for Eu^{3+} in LuF_3 was not found; a value of 8.0 eV was tentatively assumed. It is based on the value for the other three REF_3 compounds, and on the trend of larger CT energy with a smaller size of the host lattice site.[22] Similarly a value of 8.2 eV was assumed for $LiLuF_4$. In the case of PbF_2, CdF_2, and Al_2O_3, information on E^{CT} is not available. For $LuAlO_3$, the Eu^{3+} CT energy is derived from the 5.58 eV CT energy of Yb^{3+} in $LuAlO_3$.[32]

The value for $U(6,A)$ in column 8 of Table I can be derived by constructing a host referred binding energy scheme. Such a method, however, often cannot provide $U(6,A)$ with better accuracy than $\pm$0.2 eV. In a separate study[17] an empirical relationship between the value for $U(6,A)$ from

TABLE I. The compound dependent experimental values $E^{ex}(A)$, $E^{CT}(6,3+,A)$, $D(3+,A)$, and $U(6,A)$ required for construction of the VRBE schemes. The energy $E_V(A)$ at the top of the valence band is obtained by applying the chemical shift model. All energies are in eV. Estimated values are in italic font.

A	$E^{ex}(A)$	Ref. (E^{ex})	E^{CT}(Eu)	Ref. (E^{CT})	$D(3+,A)$	Ref. (D)	$U(6,A)$	$E_V(A)$
LaF_3	10.4	22,54	7.43	22	1.08	23	7.51	−11.8
GdF_3	*10.9*		7.75	55	1.11	56,57	*7.56*	−12.1
YF_3	11.3	22,58,59	7.90	22	1.21	23	7.50	−12.2
LuF_3	11.4	60,61	*8.00*		1.29	23	7.56	−12.4
$LiGdF_4$	10.9	62	8.00	63,64	1.89	23	*7.56*	−12.4
$LiYF_4$	11.0	22,61,65	8.09	22	1.84	23	7.52	−12.4
$LiLuF_4$	11.4	61	*8.20*		1.89	23	7.51	−12.5
BaF_2	10.0	66–68	7.70	69	1.87	23	7.38	−12.0
SrF_2	10.6	66,68,70,71	7.90	69	1.89	23	7.32	−12.1
CaF_2	11.1	22	8.10	22,69,72	2.04	23	7.31	−12.3
$LiCaAlF_6$	12.1	73–75	8.05	76	1.57	23,77	7.65	−12.5
CdF_2	*7.80*	78,79	–		2.20	–	*7.45*	−12.3
PbF_2	5.70	80–82	–		1.97	80	*7.37*	−10.1
Al_2O_3	9.00	24,83,84	–		2.44	39	*7.06*	−9.80
$SrAl_{12}O_{19}$	7.90	29,30,85	4.13	86	1.37	23	7.06	−8.23
$LaMgAl_{11}O_{19}$	*7.55*	25–28	4.28	25,87	1.53	23	7.05	−8.38
$LaAlO_3$	*5.90*	22,88	3.91	22,89,90	2.21	23	6.67	−7.85
$GdAlO_3$	*7.40*	22,91–93	4.71	22,90,92	2.08	23,94	6.75	−8.66
$YAlO_3$	7.96	22,95–97	5.06	22,98,99	2.05	23	6.81	−9.04
$LuAlO_3$	8.35	32,100–102	*5.18*	32	2.11	23	6.83	−9.17
$Lu_3Al_5O_{12}$	7.35	46	5.65	46	3.35	46	6.77	−9.60
$Y_3Al_5O_{12}$	7.10	46	5.42	46	3.41	46	6.77	−9.38
$Y_3Al_2Ga_3O_{12}$	6.50	46	5.19	46	3.27	46	*6.77*	−9.14
$Y_3Ga_5O_{12}$	6.10	46	5.05	46	3.22	46	*6.77*	−9.01
$Gd_3Ga_5O_{12}$	6.00	46	5.00	46	3.22	46	*6.77*	−8.96
$Lu_3Ga_5O_{12}$	6.00	46	5.00	46	3.08	46	*6.77*	−8.96
AlN-wurtzite	6.20	51,52	3.49	51,52	3.81	51,52	*6.40*	−7.27
GaN-wurtzite	3.48	51,52	3.15	51,52	–	–	*6.30*	−6.89

constructed HRBE schemes and the centroid shift $\epsilon_c(A)$ of the $5d$ configuration of Ce^{3+} was established. The centroid shift (in eV) is defined as[33]

$$\epsilon_c(A) = 6.35 - \tfrac{1}{5}\Sigma_{i=1}^{5} E_{fd_i}(1,3+,A), \quad (4)$$

where 6.35 eV is the average energy of the five $5d$ levels above the $4f$-ground state in the free Ce^{3+} ion, and $E_{fd_i}(1,3+,A)$ are the energy of the five $4f$-$5d$ transitions for Ce^{3+} in a chemical environment A. Both the centroid shift and the Coulomb repulsion energy are determined by the properties of the anion ligands around the lanthanide impurity, and the relationship between them could be functionalized as[17]

$$U(6,A) = 5.44 + 2.834e^{\epsilon_c(A)/2.2}. \quad (5)$$

Data on the centroid shift with ±0.05 eV accuracy are available for Ce^{3+} in about 150 different compounds.[33,34] One may now use the accurate value for the centroid shift to derive the value for $U(6,A)$ using Eq. (5). In Table I the thus derived $U(6,A)$ values are listed. For the compounds where the centroid shift $\epsilon_c(A)$ is not known, one has to determine $U(6,A)$ from the constructed HRBE scheme. Since both the centroid shift and $U(6,A)$ change in a very systematic fashion with the composition of the compound,[33] one may also estimate $U(6,A)$ fairly well.

Column 6 of Table I compiles the redshift $D(3+,A)$ of the Ce^{3+} $4f$-$5d_1$ excitation band defined as

$$D(3+,A) = 6.12 - E_{fd_1}(1,3+,A), \quad (6)$$

where $E_{fd_1}(1,3+,A)$ is the lowest energy $4f$-$5d$ transition of Ce^{3+}, and 6.12 eV is that same energy for the free Ce^{3+} ion. A compilation on redshift values comprising more than 300 different compounds appeared in Refs. 23 and 35. Since publication of that work better data became available, and if so in Table I those values are listed with the references. The redshift $D(3+,CdF_2)$ has been estimated from $D(2+,CdF_2) = 1.17$ eV for Eu^{2+} in CdF_2[36,37] utilizing the linear relationship between both types of redshift values that were established in Ref. 38. In the case of Al_2O_3 the redshift was derived from the energy of the first Tb^{3+} spin allowed $4f$-$5d$ transition from the work of Zhu *et al.*[39] Similarly, the redshift for AlN was obtained from Pr^{3+} and Tb^{3+} data. The redshift in GaN is not known.

IV. RESULTS AND DISCUSSION

The abundance of data that is available on $E^{CT}(6,3+,A)$, $E^{ex}(A)$, and that can be obtained for $U(6,A)$, combined with Eq. (1) provide a tool not only to establish $4f$ VRBEs of lanthanide impurities but also to determine $E_V(A)$ and $E_C(A)$ of the inorganic or organic host compound. Figure 3

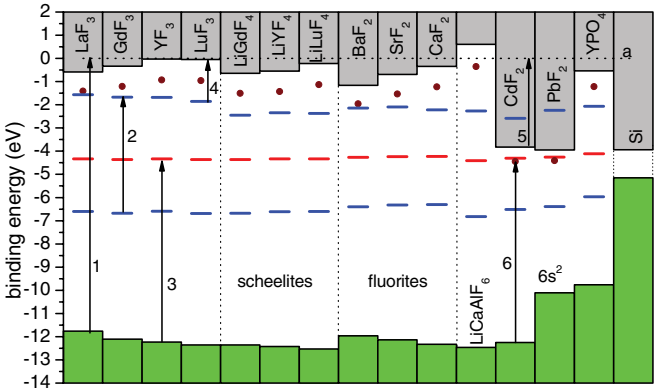

FIG. 3. (Color online) Vacuum referred binding energies in various fluoride compounds. Arrows 1 to 6 indicate the work function Φ, $E_{fd_1}(Ce^{3+})$, $E^{CT}(Eu^{3+})$, $E_{dC}(Ce^{3+})$, the electron affinity $\chi(A)$, and the exciton creation energy E^{ex}, respectively. E_V and E_C for Si are shown for comparison. Dashed horizontal line a is the vacuum level.

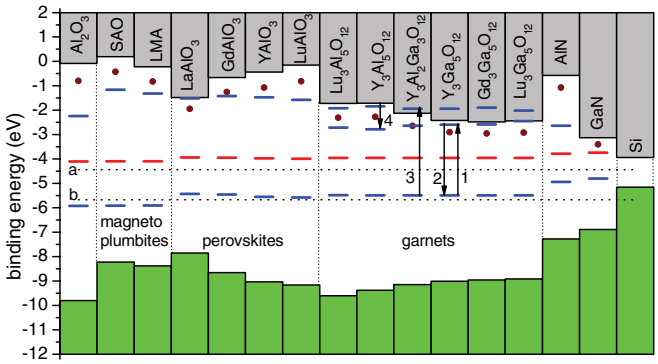

FIG. 4. (Color online) Binding energies in aluminate and gallate compounds. For the garnet compounds also the $5d_2$-VRBE level of Ce^{3+} is shown. The dashed horizontal lines a and b indicate the -4.44 eV H_2/H^+ and -5.67 eV OH^-/O_2 reduction potentials for water splitting relative to the vacuum energy. SAO $= SrAl_{12}O_{19}$ and LMA $= LaMgAl_{11}O_{19}$.

demonstrates results for various fluoride compounds. The $4f$ VRBE of Eu^{2+}, the $4f$ VRBE of Ce^{3+}, and the $5d_1$ VRBE of the electron in the lowest energy $5d$ state of Ce^{3+} are shown by horizontal bars (levels). The solid data symbols show the binding energy $E_X \equiv E_V + E^{ex}$ of the electron in the host exciton state. The $4f$ VRBE for Eu^{2+} appears always within 0.1 eV from -4.3 eV. Subtracting $E^{CT}(6,3+,\text{fluoride})$, which is typically 8 eV in fluoride compounds (see Fig. 2 and arrow 3 in Fig. 3), brings E_V(fluorides) near -12 eV, which agrees with XPS results.[5–7] There are small but significant and systematic variations in E_V. Variations that will be hard or impossible to observe with photoelectron spectroscopy techniques because of limited accuracy. E_V of the REF_3 (RE = La, Gd, Y, Lu) compounds shows a slight decrease from -11.8 to -12.4 eV when the size of the lanthanide ion decreases from La^{3+} to Lu^{3+}. A similar trend is observed for the scheelites $LiREF_4$, and the AEF_2 (AE = Ba, Sr, Ca) compounds with fluorite structure. The energy E_C behaves opposite; it increases with the smaller size of the cation. This is all a manifestation of the Madelung potential in highly ionic compounds that raises E_C and lowers E_V when the lattice parameter decreases. In the very wide band gap compound $LiCaAlF_6$, the chemical shift model applied to the available spectroscopic data even leads to a negative electron affinity of -0.6 eV.

The energy difference E_{dC} between E_C and the Ce^{3+} $5d_1$ VRBE (see arrow 4 in Fig. 3) determines the stability of $5d_1$-$4f$ emission against quenching by thermal ionization of the $5d$ electron to the conduction band. Such quenching starts already at room temperature in LaF_3 but emission is stable up to 900 K in $LiYF_4$,[40] which is all consistent with the level locations in Fig. 3. This all provides evidence that the tool presented in this work based on Eq. (1) provides electronic schemes consistent with observation. For CdF_2 and PbF_2 there is not enough spectroscopic data to construct a $4f$-HRBE scheme. However, one may proceed differently by employing the gained knowledge that the $4f$ VRBE for Eu^{2+} must be close to -4.3 eV; the typical value for fluoride compounds. By further using that the Eu^{2+} EPR signal in CdF_2:Eu disappears due to thermal ionization of Eu^{2+} with a 0.35 eV activation energy barrier,[36] one arrives at $E_C \approx -3.9$ eV. This value is in excellent agreement with the known electron affinity (see arrow 5) of 4.0 eV.[41] Next with $E^{ex} = 7.8$ eV[42] (arrow 6) one arrives at $E_V = -12.3$ eV, which is close to that of CaF_2 and agrees well with XPS data.[5] Eu enters PbF_2 as trivalent and only after prolonged x-ray irradiation at 77 K can it be reduced to Eu^{2+} evidenced by a characteristic Eu^{2+} EPR signal.[43] This suggests that the Eu^{2+} level is even closer to E_C than in CdF_2, which brings in Fig. 3 E_C near -4 eV. Finally, with $E^{ex} = 5.7$ eV, the top of the valence band must be situated at -10.1 eV. Again there is excellent consistency with XPS studies on PbF_2 and $Cd_{1-x}Pb_xF_2$ mixed compounds, where the Pb^{2+} $6s^2$ valence band is found $\approx$2.3 eV above the $2p^6$ F^- valence band.[5,44] Figure 3 now reveals that the $5d_1$ VRBE for Ce^{3+} (and also for all other divalent and trivalent lanthanides) in CdF_2 and PbF_2 is well above E_C; indeed lanthanide $5d$-$4f$ emission is never observed in these compounds. CdF_2 and PbF_2 very nicely demonstrate how information from photoelectron spectroscopy, optical spectroscopy, and EPR can be combined to establish the electronic structure. The conclusion is that Eq. (1) applied to fluoride compounds provides values for E_V and E_C that are fully consistent with what is experimentally known from XPS techniques.

To demonstrate that Eq. (1) applies equally well to compounds other than the highly ionic fluorides, Fig. 4 shows binding energies in various aluminate and gallate compounds. For the oxides, the Eu^{2+} $4f$ VRBE is near -4.0 eV, and E_V varies between -9.7 and -7.8 eV. The 2 to 4 eV difference with the fluoride compounds is all consistent with the well-known fact that electrons in the O^{2-} $2p^6$-valence band are less strongly bonded than those in F^-. The rare earth (pseudo)-perovskites $REAlO_3$ (RE = La, Gd, Y, Lu) demonstrate like in Fig. 3 the trend that E_V decreases and E_C increases with a decrease of RE size. Because the $5d_1$ VRBE for Ce^{3+} appears rather constant, E_{dC} increases and the emission from the Ce^{3+} $5d_1$ level becomes more stable against thermal quenching; indeed there is no Ce^{3+} emission in $LaAlO_3$, quenching starts near room temperature in $GdAlO_3$, and it is very temperature stable in $YAlO_3$.[40,45] The value of -7.8 eV for $E_V(LaAlO_3)$ is

independently confirmed by the value of −8.1 eV from Ref. 9; the difference is within error margins.

The aluminum and gallium compounds with garnet crystal structure form a family of compounds that is very important for luminescent devices, and there are many ongoing studies to develop improved LED phosphors and scintillators. In Ref. 46 a review on the spectroscopic properties of the $RE_3Al_{1-x}Ga_xO_{12}$ (RE = Gd, Y, Lu; $x = 0, 0.2, 0.4, 0.6, 0.8, 1.0$) garnet compounds was presented, and also electronic structure schemes were made using the chemical shift model. Some of those results are shown in Fig. 4. They demonstrate a relatively large electron affinity of 2 to 2.5 eV in the garnet compounds. Comparing $Y_3Al_5O_{12}$, $Y_3Al_2Ga_3O_{12}$, and $Y_3Ga_5O_{12}$, one observes that E_C lowers and approaches the $5d_1$ VRBE of Ce^{3+} closer. This is consistent with recent photoconductivity studies by Ueda *et al.*[4] At room temperature a photocurrent is generated on exciting (see arrow 1) the $5d_1$ level of Ce^{3+} in $Y_3Ga_5O_{12}$. Although $5d_1$-$4f$ emission (arrow 2) is observed with decay time of 45 ns,[47] the $5d_1$ VRBE is sufficiently close below E_C to create a photocurrent by thermal ionization. This does not occur anymore in $Y_3Al_2Ga_3O_{12}$, and here the second $5d_2$ level at energy well above E_C needs to be excited (arrow 3). In $Y_3Al_5O_{12}$ even excitation of the $5d_2$ level does not generate a photocurrent. Probably a very short lifetime (<0.1 ns) of the $5d_2$ level due to phonon relaxation to the $5d_1$ level (arrow 4) prevents efficient thermal ionization. The garnets $Gd_3Ga_5O_{12}$ and $Lu_3Ga_5O_{12}$ show level locations quite similar to $Y_3Ga_5O_{12}$, but even a 0.1 eV binding energy difference has strong consequences. For $Gd_3Ga_5O_{12}$ and $Y_3Ga_5O_{12}$, Ce^{3+} emission can be observed although it is already severely quenched at room temperature; for $Lu_3Ga_5O_{12}$ emission is fully absent.

The level energies for the two compounds with magnetoplumbite structure are added because they show a large (≈4.7 eV) $4f$-$5d_1$ energy difference which is caused by an exceptionally small crystal field splitting of the $5d$ states. On the other hand, in the garnets, crystal field splitting is exceptionally large leading to small $4f$-$5d_1$ energy difference and relatively long wavelength (≈550 nm) Ce^{3+} emission (arrow 2). For Al_2O_3 one may use $E_V = -9.8$ eV from Ref. 9 and with E^{ex} from optical studies then E_C is found at −0.1 eV. Although sufficient spectroscopic information of lanthanides in Al_2O_3 to construct a VRBE scheme is not yet available, one may already predict it quite well by taking $U(6,A)$ similar to that for the magnetoplumbites.

Many studies, both experimental and theoretical, on establishing E_V and E_C of AlN and GaN and the band offsets at AlN/GaN heterojunctions have appeared (see, e.g., Ref. 48 and references therein). Activated with lanthanides these compounds are of much interest to develop the next generation of lighting systems with even better energy efficiency than that of LED phosphors.[49,50] $4f$ HRBE schemes for the lanthanides in these compounds were published in Refs. 51 and 52. Together with revisions suggested in Ref. 3 and the ideas from the chemical shift model, they can be converted into $4f$-VRBE schemes resulting in the level energies on the right-hand side in Fig. 4. The difference of 0.4 eV between E_V(AlN) and E_V(GaN) agrees with experimental and theoretical values obtained independently.[48] Again Eq. (1) proposed in Ref. 16 provides VRBE schemes that are fully consistent with available experimental data.

V. SUMMARY AND CONCLUSIONS

Figures 3 and 4 provide only a small cross section through the family of inorganic compounds and only with the levels for Eu^{2+} and Ce^{3+}. Yet, the data provided for each compound are sufficient to generate a $4f$-VRBE scheme with the full richness of information as in Fig. 1. Such schemes predict and explain electron transfer phenomena between a lanthanide impurity state and host states, and from one lanthanide impurity to another. Luminescence quenching, charge carrier storage, photochromic properties, and photoconductivity are all determined by such electron transfer. The past 5 years show an increased research activity on compounds doped with two different lanthanide ions, and then those schemes are important to make a proper interpretation of the results; they even enable deliberate design.[14]

A HRBE scheme is constructed by cross-relating data pertaining to different lanthanides in the same compound, and by exploiting the universal shape of the double zigzag binding energy curves in Fig. 1. A VRBE scheme is then constructed utilizing the $U(6,A)$ value from that HRBE scheme, or obtained otherwise, and exploiting Eq. (1). This has been done for the 28 compounds of Figs. 3 and 4 but can be done for all 500 compounds of Fig. 2, and by utilizing spectroscopic information other than E^{CT} data can be done for many more compounds; the data needed are already available. With Figs. 3 and 4 some trends with structural and chemical properties were briefly addressed. The purpose and challenge is to arrive at a collection of binding energy schemes pertaining to about, say, 1000 different insulators and semiconductors that is consistent with available data from different disciplines of science. The data and trends in E_V and E_C with composition and structure can then provide guidance in the search for compounds with desired electronic properties like in the field of thin film heterojunctions with, e.g., Si, and in the field of photoelectrochemical cells for water splitting. As illustrated, the binding energies $E_V(\mathrm{Si}) = -5.15$ eV[53] and E_C(Si) for pure silicon and the relevant reduction potentials for water splitting are shown by the dashed lines a and b in Fig. 4.

Now that a method to generate a $4f$-VRBE scheme for lanthanide doped compounds is available, one may start to develop similar models and methods to determine the VRBE of other impurities like actinides with partly filled $5f$ shells, transition metal elements with partly filled d shells, and Tl^+, Pb^{2+}, and Bi^{3+} with a filled outer $6s^2$ shell. This is a more challenging task because the d-shell and s-shell electrons are less contracted and less shielded than f-shell electrons are, and they will have more complicated interactions with the chemical environment. Nevertheless, it will be extremely interesting to have knowledge on where to expect the VRBEs of electrons in transition metal or $6s^2$ impurity states with respect to that in the lanthanide states. One may then better understand and predict properties of compounds activated with, for example, a lanthanide together with a transition metal element; a functional materials research field that is largely unexplored.

[1] E. Malguth, A. Hofmann, and M. R. Phillips, Phys. Status Solidi B **245**, 455 (2008).
[2] C. W. Thiel and R. L. Cone, J. Lumin. **131**, 386 (2011).
[3] P. Dorenbos, A. H. Krumpel, E. van der Kolk, P. Boutinaud, M. Bettinelli, and E. Cavalli, Opt. Mater. **32**, 1681 (2010).
[4] J. Ueda, S. Tanabe, and T. Nakanishi, J. Appl. Phys. **110**, 053102 (2011).
[5] R. T. Poole, J. Liesegang, R. C. G. Leckey, J. G. Jenkin, and J. B. Peel, Phys. Rev. B **13**, 896 (1976).
[6] R. T. Poole, J. Szajman, R. C. G. Leckey, J. G. Jenkin, and J. Liesegang, Phys. Rev. B **12**, 5872 (1975).
[7] W. Pong and C. S. Inouye, Opt. Soc. Am. **68**, 521 (1978).
[8] I. Vurgaftman, J. R. Meyer, and L. R. Ram-Mohan, J. Appl. Phys. **89**, 5815 (2001).
[9] J. Robertson, K. Xiaong, and S. J. Clark, Thin Solid Films **496**, 1 (2006).
[10] J. Robertson and K. Xiaong, Opt. Appl. Phys. **106**, 313 (2007).
[11] R. van de Krol, Y. Liang, and J. Schoonman, J. Mater. Chem. **18**, 2311 (2008).
[12] T. Bak, J. Nowotny, M. Rekas, and C. C. Sorrell, Int. J. Hydrogen Energy **27**, 991 (2002).
[13] E. Rogers, P. Dorenbos, and E. van der Kolk, New J. Phys. **12**, 093038 (2011).
[14] P. Dorenbos, J. Mater. Chem. **22**, 22344 (2012).
[15] P. Dorenbos, ECS J. Solid State Sci. Technol. **2**, R3001 (2013).
[16] P. Dorenbos, Phys. Rev. B **85**, 165107 (2012).
[17] P. Dorenbos, J. Lumin. **136**, 122 (2013).
[18] M. J. Caldas, A. Fazzio, and A. Zunger, Appl. Phys. Lett. **45**, 671 (1984).
[19] J. M. Langer and H. Heinrich, Phys. Rev. Lett. **55**, 1414 (1985).
[20] C. Delerue and M. Lannoo, Phys. Rev. Lett. **67**, 3006 (1991).
[21] J. M. Langer, Mater. Sci. Forum **143–147**, 721 (1994).
[22] P. Dorenbos, J. Lumin. **111**, 89 (2005).
[23] P. Dorenbos, J. Lumin. **91**, 155 (2000).
[24] R. H. French, J. Am. Ceram. Soc. **73**, 477 (1990).
[25] J.-Z. Xu, Z.-H. Zhang, and Y.-H. Wang, Chin. J. Inorganic Chem. **5**, 913 (2006).
[26] W. B. Im, Y.-H. Won, Y.-I. Kim, H. S. Jang, and D. Y. Jeon, Electron. Mater. Lett. **2**, 1 (2006).
[27] X. Wang, T. Pan, T. Zang, J. Li, Z. Zhao, L. Zhang, and J. Xu, Sci. China Ser. E Tech. Sci. **52**, 3678 (2009).
[28] M. L. H. ter Heerdt, E. van der Kolk, W. M. Yen, and A. M. Srivastava, J. Lumin. **100**, 107 (2002).
[29] P. A. Rodnyi, P. Dorenbos, G. B. Stryganyuk, A. S. Voloshinovskii, A. S. Potapov, and C. W. E. van Eijk, J. Phys.: Condens. Matter **15**, 719 (2003).
[30] V. B. Mikhailik and H. Kraus, Spectrosc. Lett. **43**, 350 (2010).
[31] Z. Zhang, Y. Zhang, X. Li, J. Xu, and Y. Huang, J. Non-Cryst. Solids. **354**, 1943 (2008).
[32] I. Kamenskikh, C. Pedrini, A. Petrosyan, and A. Vasil'ev, J. Lumin. **129**, 1509 (2009).
[33] P. Dorenbos, J. Lumin. **135**, 93 (2013).
[34] P. Dorenbos, Phys. Rev. B **65**, 235110 (2002).
[35] P. Dorenbos, J. Lumin. **91**, 91 (2000).
[36] M. Godlewski, D. Hommel, J. M. Langer, and H. Przybylinska, J. Lumin. **24/25**, 217 (1981).
[37] P. Dorenbos, J. Lumin. **104**, 239 (2003).
[38] P. Dorenbos, J. Phys.: Condens. Matter. **15**, 4797 (2003).
[39] Z. Zhu, D. Liu, H. Liu, G. Li, J. Du, and Z. He, J. Lumin. **132**, 261 (2012).
[40] L.-J. Lyu and D. S. Hamilton, J. Lumin. **48&49**, 251 (1991).
[41] B. A. Orlowski and J. M. Langer, Phys. Status Solidi B **91**, K53 (1979).
[42] J. P. Albert, C. Jouanin, and C. Gout, Phys. Rev. B **16**, 4619 (1977).
[43] N. Guskos, J. Kuriata, I. H. Salikhov, N. I. Silkin, and S. Yagadin, Phys. Status Solidi B **115**, K133 (1983).
[44] V. Chab, B. Kowalski, and B. A. Orlowski, Solid State Commun. **58**, 667 (1986).
[45] E. van der Kolk, J. T. M. de Haas, A. J. J. Bos, C. W. E. van Eijk, and P. Dorenbos, J. Appl. Phys. **101**, 083703 (2007).
[46] P. Dorenbos, J. Lumin. **134**, 310 (2013).
[47] X. Liu, X. Wang, and W. Shun, Phys. Status Solidi A **101**, K161 (1987).
[48] P. G. Moses, M. Miao, Q. Yan, and C. G. van de Walle, J. Chem. Phys. **134**, 084703 (2011).
[49] Y. Q. Wang and A. J. Steckl, Appl. Phys. Lett. **82**, 502 (2003).
[50] W. M. Jadwisienczak, H. J. Lozykowski, A. Xu, and B. Patel, J. Electron. Mater. **31**, 776 (2002).
[51] P. Dorenbos and E. van der Kolk, Opt. Mater. **30**, 1052 (2008).
[52] P. Dorenbos and E. van der Kolk, Appl. Phys. Lett. **89**, 061122 (2006).
[53] G. W. Gobeli and F. G. Allen, Phys. Rev. **127**, 141 (1962).
[54] E. D. Thoma, H. Shields, Y. Zhang, B. C. McCollum, and R. T. Williams, J. Lumin. **71**, 93 (1997).
[55] S. P. Feofilov, Y. Zhou, J. Y. Jeong, D. A. Keszler, and R. S. Meltzer, J. Lumin. **122-123**, 503 (2006).
[56] S. H. M. Poort, A. Meyerink, and G. Blasse, Solid State Commun. **103**, 537 (1997).
[57] M. Kobayashi, R. Nakamura, M. Ishi, N. Solovieva, and M. Nikl, Jpn. J. Appl. Phys. **42**, 1648 (2003).
[58] V. Pankratov, M. Kirm, and H. von Seggern, J. Lumin. **113**, 143 (2005).
[59] D. N. Karimov, E. A. Krivandina, Z. I. Zhmurova, B. P. Sobolev, V. A. Bezhanov, S. P. Chernov, and G. M. Shapochkin, Crystallogr. Rep. **51**, 1009 (2006).
[60] M. Kirm, G. Stryganyuk, S. Vielhauer, G. Zimmerer, V. N. Makhov, B. Z. Malkin, O. V. Solovyev, R. Y. Abdulsabirov, and S. L. Korableva, Phys. Rev. B **75**, 075111 (2007).
[61] N. Yu. Kirikova, M. Kirm, J. C. Krupa, V. N. Makhov, E. Negodin, and J. Y. Gesland, J. Lumin. **110**, 135 (2004).
[62] M. Kirm, J. C. Krupa, V. N. Makhov, M. True, S. Vielhauer, and G. Zimmerer, Phys. Rev. B **70**, 241101 (2004).
[63] R. T. Wegh, H. Donker, K. D. Oskam, and A. Meijerink, J. Lumin. **82**, 93 (1999).
[64] S. Lepoutre, D. Boyer, and R. Mahiou, J. Lumin. **128**, 635 (2008).
[65] E. Negodin, "Inter- and intraconfigurational luminescence of LiYF4:Er^{3+} under selective VUV excitations," thesis, University of Hamburg, Germany, 2003.
[66] T. Tomiki and T. Miyata, J. Phys. Soc. Jpn. **27**, 658 (1969).
[67] E. Radzhabov, A. I. Nepomnyashikh, and A. Egranov, J. Phys.: Condens. Matter **14**, 7337 (2002).
[68] G. W. Rubloff, Phys. Rev. B **5**, 662 (1972).
[69] E. Radzhabov and A. Nepomnyashchikh, Solid State Commun. **146**, 376 (2008).
[70] K. V. Ivanovskikh, V. A. Pustovarov, and B. V. Shulgin, Nucl. Instrum. Methods A **543**, 229 (2005).
[71] K. V. Ivanovskikh, V. A. Pustovarov, B. V. Shulgin, and M. Kirm, Phys. Solid State **47**, 1446 (2005).
[72] P. A. Rodnyi, A. Kh Khadro, A. S. Voloshinovskii, and G. B. Stryganyuk, Opt. Spectrosc. **103**, 568 (2007).

[73]M. Henke, "Interkonfigurale Übergänge Lanthanid-dotierter Kristalle," thesis, Hamburg University, Germany, 2001.
[74]K. Shimamura, H. Sato, A. Bensalah, V. Sudesh, H. Machida, N. Sarukura, and T. Fukuda, Cryst. Res. Technol. **36**, 801 (2001).
[75]M. Kirm, M. True, S. Vielhauer, G. Zimmerer, N. V. Shiran, I. Shpinkov, D. Spassky, K. Shimamura, and N. Ichinose, Nucl. Instrum. Methods A **537**, 291 (2005).
[76]M. Kirm, Y. Chen, S. Neicheva, K. Shimamura, N. Shiran, M. True, and S. Vielhauer, Phys. Status Solidi C **2**, 418 (2005).
[77]T. Tsuboi, V. Petrov, F. Noack, and K. Shimamura, J. Alloys Compd. **323**, 688 (2001).
[78]C. Raisin, J. M. Berger, S. Robin-Kandare, G. Krill, and A. Amamou, J. Phys. C **13**, 1835 (1980).
[79]B. A. Orlowski and O. Olenkiewicz, Phys. Status Solidi B **126**, 285 (1984).
[80]G.-H. Ren, D.-Z. Shen, S.-H. Wang, and Z.-W. Yin, Chin. Phys. Lett. **18**, 976 (2001).
[81]G. Liidja and Vl. Plekhanov, J. Lumin. **6**, 71 (1973).
[82]M. Fujita, M. Itoh, Y. Bokumoto, H. Nakagawa, D. L. Alov, and M. Kitaura, Phys. Rev. B **61**, 15731 (2000).
[83]W. C. Wong, D. S. McClure, S. A. Basun, and M. R. Kokta, Phys. Rev. B **51**, 5682 (1995).
[84]A. Lushchik, M. Kirm, Ch. Lushchik, I. Martinson, and G. Zimmerer, J. Lumin. **87–89**, 232 (2000).
[85]Z. Zhang, Y. Zhang, X. Li, J. Xu, and Y. Huang, J. Lumin. **128**, 476 (2008).
[86]S. Chawla and A. Yadav, Mater. Chem. Phys. **122**, 582 (2010).
[87]R. Zha, Z. Q. Zhao, and Z. G. Wang, Sci. Sin. Chim. **40**, 331 (2010).
[88]S-G. Lim, S. Kriventsov, T. N. Jackson, J. H. Haeni, D. G. Schlom, A. M. Balbashov, R. Uecker, P. Reiche, J. L. Freeouf, and G. Lucovsky, J. Appl. Phys. **91**, 4500 (2002).
[89]Z.-y. Mao, D.-j. Wang, Q.-f. Lu, W.-h. Yu, and Z.-h. Yuan, Chem. Commun. **3**, 346 (2009).
[90]X. Dong, X. Cui, Z. Fu, S. Zhou, S. Zhang, and Z. Dai, Mater. Res. Bull. **47**, 212 (2012).
[91]J. W. M. Verweij, M. Th. Cohen-Adad, D. Bouttet, H. Lautesse, and C. Pédrini, Chem. Phys. Lett. **239**, 51 (1995).
[92]Y. Wang, X. Guo, T. Endo, Y. Murakami, and M. Ushirozawa, J. Solid State Chem. **177**, 2242 (2004).
[93]Y. Wang and H. Gao, Electrochem. Solid State Lett. **9**, H19 (2006).
[94]E. van der Kolk, P. Dorenbos, J. T. M. de Haas, and C. W. E. van Eijk, Phys. Rev. B **71**, 045121 (2005).
[95]T. Tomiki, M. Kaminao, Y. Tanahara, T. Futemma, M. Fujisawa, and F. Fukudome, J. Phys. Soc. Jpn. **60**, 1799 (1991).
[96]V. Babin, M. Kink, Y. Maksimov, K. Nejezchleb, M. Nikl, and S. Zazubovich, J. Lumin. **122-123**, 332 (2006).
[97]Yu. V. Zorenko, A. S. Voloshinovskii, G. M. Stryganyuk, and I. V. Konstankevych, Opt. Spectrosc. **96**, 70 (2004).
[98]L. Wang, Y. Wang, and H. Gao, J. Electrochem. Soc. **153**, G943 (2006).
[99]H. Gao and Y. Wang, Mater. Res. Bull. **42**, 921 (2007).
[100]L. Zhang, C. Madej, C. Pedrini, B. Moine, C. Dujardin, A. Petrosyan, and A. N. Belsky, Chem. Phys. Lett. **268**, 408 (1997).
[101]C. Dujardin, C. Pedrini, J. C. Gacon, A. G. Petrosyan, A. N. Belsky, and A. N. Vasil'ev, J. Phys.: Condens. Matter **9**, 5229 (1997).
[102]A. J. Wojtowicz, *Proceedings of the International Conference on Inorganic Scintillators and Their Applications* (Delft University Press, The Netherlands, 1996), p. 95.